B.D. NECHYPORUK,[1] O.F. KOLOMYS,[2] B.P. RUDYK,[3] V.V. STRELCHUK,[2]
M.V. MOROZ,[3] V.O. MYSLINCHYK,[1] B.A. TATARYN [4]

[1] Rivne State Humanitarian University
 (31, Plastova Str., Rivne 33028, Ukraine)
[2] V.E. Lashkaryov Institute of Semiconductor Physics, Nat. Acad. of Sci. of Ukraine
 (41, Nauky Ave., Kyiv 03028, Ukraine)
[3] National University of Water Management and Nature Resources
 (11, Soborna Str., Rivne 33028, Ukraine; e-mail: b.p.rudyk@nuwm.edu.ua)
[4] Lesya Ukrainka Volyn National University
 (13, Volya Ave., Luts'k 43025, Ukraine)

OPTICAL AND STRUCTURAL PROPERTIES OF NANOPOWDERS OF LEAD COMPOUNDS OBTAINED BY THE ELECTROCHEMICAL METHOD

The influence of the temperature and electrolyte composition on the synthesis of nanopowders of lead compounds using the electrochemical method has been studied. X-ray diffraction (XRD) studies were carried out, and their results are used to determine the composition of obtained specimens and the size of nanocrystallites in them (using the Debye–Scherrer formula). The possibility of the formation of lead oxides and lead carbonate, when electrochemically synthesizing nanoparticles is discussed. It is shown that a mixture of lead oxide and lead carbonate nanocrystals is obtained irrespective of the electrolyte temperature. The results of XRD structural studies are compared with the results of Raman studies of the same specimens. The photoluminescence bands of synthesized compounds are analyzed.

K e y w o r d s: α- and β-lead oxides, lead carbonate, XRD structural studies, nanoparticle size, Debye–Scherrer formula, Raman scattering, photoluminescence.

1. Introduction

Lead belongs to chemical elements with a relatively high atomic mass. Therefore, it has been used for a long time in the manufacture of protection elements against radioactive emissions and X-rays and as a material for protective containers for the storage and transportation of radioactive materials. Lead oxides are traditionally used for producing radiation-resistant glasses and sitals. Despite the toxicity of lead [1], it and its compounds are widely used in semiconductor electronics.

Since the mid-1990s, a permanent growth of the interest of materials scientists in semiconductor materials in the nanostructured form has been observed, because the properties of such materials can substantially differ from those of bulk ones [2,3], which opens new horizons for the applications of these materials.

PbO-based nanoparticles are used as functional materials in various sensors; as a material for power cell electrodes, lithium batteries [4], and fuel cells; and as efficient reusable catalysts, dyes, and phosphors [5–7]. The scope of PbO applications is expanded by the existence of two polymorphic phases, α-PbO and β-PbO, which are different in their structural and optical properties. The low-temperature phase, α-PbO, has the band gap $E_g = 1.92$ eV, which allows α-PbO to be used in photovoltaics [3]. At a temperature higher than 490 °C, a transition takes place from the tetragonal α-PbO phase to the or-

thorhombic β-PbO one with $E_g = 2.7$ eV. The β-PbO phase can be used as one of the components of a transparent conductive coating in optoelectronic devices [2].

PbO is a photoactive semiconducting material. The combination of its luminescent properties and radiation stability makes it promising for the development of direct visualizers of X-ray images and other promising types of sensors, which plays an important role in both scientific [8] and medical applications. For example, it can be the construction of a 2D-3D array of X-ray detectors for high-resolution computer-aided tomography (micro-CT) based on amorphous PbO [2].

As is known, nanostructured semiconductors are obtained by applying various methods: laser gas-phase deposition, molecular beam epitaxy, synthesis in colloidal solutions, hydrothermal synthesis, chemical and electrochemical depositions, mechanochemical fragmentation, thermal/magnetron sputtering, and others [2, 3]. They all have both advantages and limitations.

When obtaining the nanostructures and nanomaterials, besides the technology itself, of great importance are the development and implementation of methods aimed at the study of and control over their dimensional and structural characteristics for producing a product of the required quality. The main methods to analyze the dispersion of particles are non-destructive optical (photoluminescence and Raman) studies and the X-ray structural analysis [9, 10].

The aim of this work was to obtain lead oxide nanoparticles using the electrolytic method and to study the influence of synthesis parameters on their optical and structural properties.

2. Experimental Part and Materials

Nanopowders of lead compounds were produced using the electrolytic method in an open glass electrolyzer with lead electrodes. A stabilized dc source (0÷15 V, 0÷5 A) was used to power the electrolyzer. As the electrolyte (in various experimental series), we used a solution of salts–sodium chloride (NaCl) and sodium carbonate ($Na_2CO_3 \times 10H_2O$)–in distilled water. The chemical purity of the reagents was not lower than the "pure for analysis" grade. The concentrations of salts in the electrolyte solutions were as follows: 0.625 g/l NaCl for the specimens in series Pb-1, Pb-4, and Pb-5; and 6.25 g/l $Na_2CO_3 \times 10H_2O$ for the specimens in

series Pb-6. The synthesis in series Pb-1, Pb-4, and Pb-5 was performed under various electrolyte temperatures from room temperature to 100 °C, and the specimens in series Pb-6 were synthesized only at a temperature of 20 °C.

The duration of the nanocrystal synthesis process was 3 h for every specimen. The current density in the electrolytic cell was $j = 1.3 \times 10^{-2}$ A/cm^2. For a steady consumption of electrode material, the direction of the direct current was reversed after each 30-min interval. After the end of the synthesis, the electrolyte was filtered using a paper filter. The resulting powder was washed in a fivefold amount of distilled water. Then the specimens were air-dried at room temperature.

X-ray studies were carried out on a DRON-4 diffractometer using CuK_α radiation, at room temperature. The diffractograms were scanned using the Bragg–Brentano ($\theta - 2\theta$) geometry. The anode voltage and the current were 41 kV and 21 mA, respectively. The diffractogram scanning increment was 0.05°, and the exposure time was 5 s.

In order to analyze the experimental diffractograms in detail, every experimental reflex was approximated by a Gaussian function. As a result, the following information was obtained: the angular position 2θ, the half-width ω (the width at the half-height), and the integrated intensity I. The obtained results were used to characterize the composition and calculate the size of nanocrystals.

The micro-Raman and micro-PL spectra of the researched powders were studied in the backscattering geometry on a Horiba Jobin-Yvon T64000 triple spectrometer equipped with an Olympus BX41 microscope. As a source of excitation of Raman spectra, the radiation of an Ar–Kr laser with a wavelength of 488.0 nm (2.54 eV) was used. With the help of a 50^x optical lens, it was focused into a spot about 1–2 μm in diameter on the specimen surface. The PL spectra were excited using the He–Cd laser radiation with a wavelength of 325 nm (3.81 eV). The signals were registered with the help of a CCD array cooled using Peltier elements.

3. Research Results

In works [11, 13], it was shown that, when fabricating cadmium sulfide and zinc oxide via the electrochemical method and at room electrolyte temperature, besides the nanocrystals of indicated compounds, the

cadmium carbonate and zinc carbonate [hydrozincite, $Zn_5(CO_3)_2(OH)_6$] compounds are also synthesized. Therefore, in this work, we obtained a reference specimen using an electrolyte solution prepared on the basis of sodium carbonate and with a high concentration of carbonate ions. Its diffractogram is shown in Fig. 1, d. By applying the known interplanar distances in lead carbonate and the Bragg equation

$$2d \sin\theta = k\lambda,$$

where d is the interplane distance, θ is the diffraction angle, k is the order of diffraction maximum, and λ is the wavelength of X-ray radiation, the angular positions of reflexes, 2θ, were calculated. The experimental parameters of reflexes were compared with the calculated ones and the data from the PDF-2 database and works [14, 15]. It was found that the diffractogram of the specimen obtained with an excess of carbonate ions (Fig. 1, d) corresponds to the X-ray standard of one of lead carbonates, cerussite $Pb_3(CO_3)_2$ $(OH)_2$, which belongs to the trigonal system, the space group $R\bar{3}m$ (No. 166).

In Fig. 1, experimental diffraction patterns of specimens obtained using the electrolytic method at various electrolyte temperatures are shown. The registered diffractograms were normalized by the peak intensity of the reflex with the angular position $2\theta = 27.20°$. From Fig. 1, one can see that all diffractograms contain reflexes characteristic of lead carbonate. This fact means that if an electrolyte on the basis of NaCl is used, a mixture of lead oxides and carbonates is obtained irrespective of the synthesis temperature. Carbon dioxide participating in the formation of lead carbonate belongs to the gases dissolved in distilled water used to prepare the electrolyte. During the synthesis process, CO_2 could also enter the electrolyte solution from air, since an open electrolytic cell was used. Under other synthesis conditions, the formation of other lead carbonates is possible; this issue requires further detailed research.

It is known [3, 7] that lead oxide can exist in two modifications: low-temperature tetragonal (α-PbO) and high-temperature orthorhombic (β-PbO) ones. The identification of oxide reflexes was carried out similarly to what was done for lead carbonate. A comparison of the experimental and calculated 2θ-values with the data taken from the PDF-2 database and works [3, 7, 15] showed that both oxide modifications are available in the specimens.
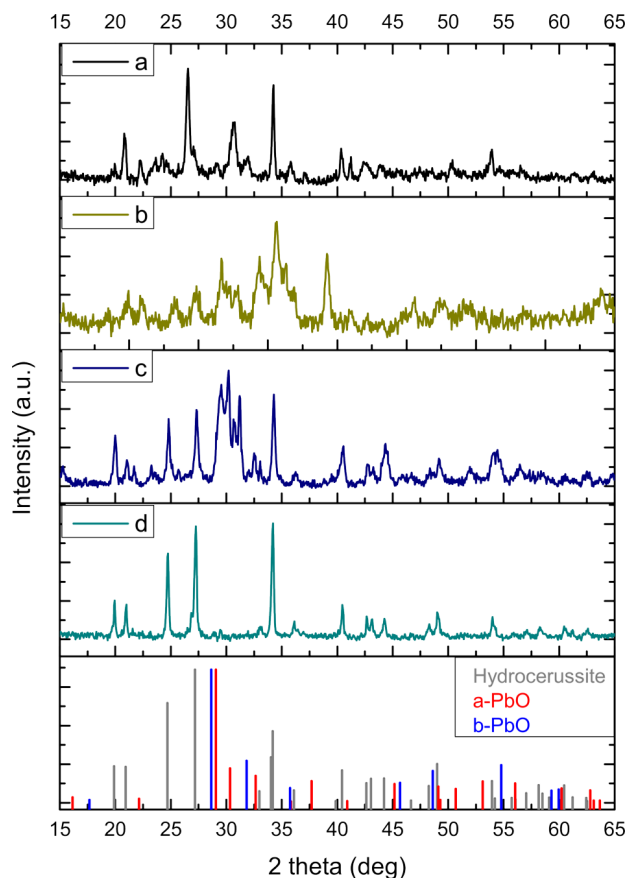
Fig. 1. X-ray diffractograms of specimens and (the bottom panel) X-ray standards of Hydrocerussite, α-PbO, and β-PbO. Synthesis parameters: NaCl electrolyte, the synthesis temperature $t = 24$ °C (a); NaCl electrolyte, $t = 60$ °C (b); NaCl electrolyte, $t = 98$ °C (c); $Na_2CO_3 \times 10H_2O$ electrolyte, $t = 20$ °C (d)

Besides the reflexes characteristic of lead carbonate, the diffractogram of the specimen obtained at a temperature of 24 °C contains reflexes of lead oxide. The most intensive of them are located within the interval of 2θ angles from 27.70° to 33.60°.

It is known that for a diffractometer with a flat specimen, the integrated intensity I of diffraction maxima is described by the formula [12]

$$I = I_0 \frac{e^4 \lambda^3 l}{32\pi m^2 c^4 R} \frac{N^2}{2\mu} \text{ PLG } p\, |F|^2,$$

where I_0 is the intensity of incident X-ray radiation, e is the elementary charge, m is the electron mass, λ is the X-ray radiation wavelength, l is the path length of the reflected beam in the counter, c is the speed of
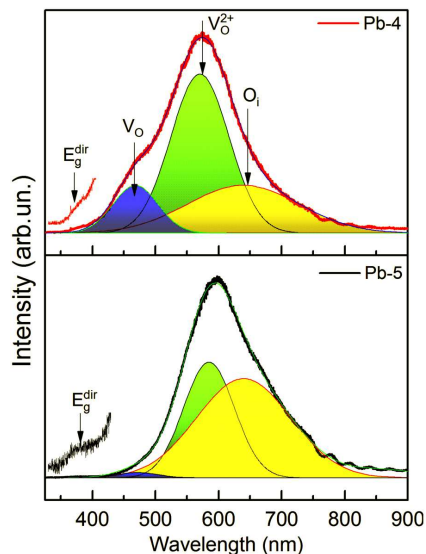
Fig. 2. Micro-PL spectra of PbO powders and the approximation of PL band by Gaussian contours; $\lambda_{exc} = 325.0$ nm, $T = 300$ K

Nanocrystal sizes in the studied specimens determined using the Debye–Scherrer method

Specimen	Electrolyte	Synthesis temperature, t, °C	D, nm		
			$PbCO_3$	α-PbO	β-PbO
Pb-4	NaCl	24	34	17	20
Pb-5	NaCl	60	29	21	21
Pb-1	NaCl	98	27	36	30
Pb-6	$NaCO_3$	20	66	–	–

light, R is the radius of goniometer, N is the number of elementary cells per unit volume, μ is the linear absorption coefficient, PLG is the angular multiplier, p is repeatability factor, and $|F|$ is the absolute value of the structural amplitude.

The formula for the integral intensity of X-ray reflexes includes the volume of the examined specimen. So, if other quantities remain unchanged, the integral intensity of the reflex is determined exclusively by the bulk content of the corresponding phase. Therefore, the integrated intensity of reflexes increases, as the volume of the components grows.

In our case, for the specimens obtained when the synthesis temperature increased (Fig. 1, *a–c*), the growth of the relative intensity of reflexes located within this angular interval was observed, which evi-

dences that the volume content of lead oxides in the studied specimens became larger.

The results obtained when processing the experimental diffraction patterns were used to calculate the sizes of nanocrystals. For this purpose, the Debye–Scherrer formula was applied [16],

$$D = \frac{0.89\,\lambda}{\beta\cos\theta},$$

where λ is the X-ray radiation wavelength, β is the half-width of the reflex, and θ is the diffraction angle. The value of the half-width β was calculated using the formula

$$\beta = \sqrt{\beta_1^2 - \beta_2^2},$$

where β_1 is the experimental value of the X-ray reflex half-width, and β_2 is its instrumental value. The instrumental values of the half-widths of X-ray reflexes were determined by analyzing the X-ray diffractograms of the reference powders of silicon and Al_2O_3, which were obtained under the same conditions. The results obtained for the size of nanocrystals in the studied specimens following the Debye–Scherrer method are quoted in Table.

From the analysis of the calculation results presented in Table, one can see that if the electrolyte on the basis of NaCl is used, and the synthesis temperature increases from 24 °C to 98 °C, the size D of the obtained lead carbonate nanoparticles decreases from 34 to 27 nm. Under the same conditions, the size of lead oxide nanocrystals increases from 17 to 36 nm for α-PbO, and from 20 to 30 nm for β-PbO. It is worth noting that the difference between the sizes of nanocrystals of both modifications (α-PbO and β-PbO) was small (only a few nanometers).

Figure 2 demonstrates the photoluminescence (PL) spectra of synthesized PbO powders (specimens Pb-4 and Pb-6); the spectra were registered at room temperature. The PL spectra of both specimens include a weak emission band at 468 nm, an intensive band at 570 nm, and a broad emission band with a maximum at 640 nm. The presence of the blue emission band at 468 nm testifies to the existence of a significant amount of lead ions Pb^{2+} in the interstitial state I_{Pb} [17, 18]. The band at 570 nm is associated with the presence of a substantial number of oxygen vacancies, which are usually located on the surface of lead

oxide microparticles, and it is a result of the recombination between holes captured by surface defects and electrons captured by the doubly ionized oxygen vacancy $V_{O_2}^{2+}$ [17, 18]. The band with a maximum at 640 nm in the orange-red spectral interval is related to interstitial oxygen in the PbO structure [18].

From the PL spectra depicted in Fig. 2, one can see that specimens Pb-4 and Pb-5 clearly demonstrate a redistribution of intensities among the emission bands of their own defects. In particular, in the case of specimen Pb-5, an intensity reduction of the band associated with interstitial lead is observed simultaneously with an increase in the amount of interstitial oxygen; the latter process may be induced by the growth of the synthesis temperature.

In addition, the PL spectrum demonstrates a very weak emission band at 385 nm, which appears due to the radiative recombination of localized excitons bound at neutral donors and/or acceptors. As was previously reported [3], lead monoxide (PbO) is a semiconductor with an indirect band gap of 1.92 eV (or 1.82 eV according to work [19]). The direct band gap width equals 3.21 eV [19, 20]. The weak intensity of the ultraviolet band associated with direct-band transitions and the increase of the defect emission band intensity testify to the concentration growth of intrinsic point defects. The difference between the intensities of the defect emission bands may arise due to a change in the size of micrograins in the PbO powders, which leads to the growth of their surface area and, accordingly, an increase in the concentration of surface non-radiative recombination centers [21].

It is known [22–24] that, depending on the temperature, pressure, or synthesis conditions, PbO can exist in various polymorphic forms: the stable tetragonal modification (α-PbO) and the orthorhombic modification (β-PbO), the latter being metastable at room temperature. By increasing the pressure, α-PbO can be transformed into β-PbO through the intermediate rhombic γ-PbO phase [25]. Therefore, in order to study the structural and crystalline quality of the synthesized PbO powders and their polymorphic forms, the corresponding vibrational spectra were measured using the Raman light scattering methods.

According to group theory, single-crystalline α-PbO belongs to the space group $P_{4/nmm}$ (D_{4h}^7). Its unit cell consists of four atoms (two PbO formula units) and has $3 \times 4 = 12$ phonon modes; three of
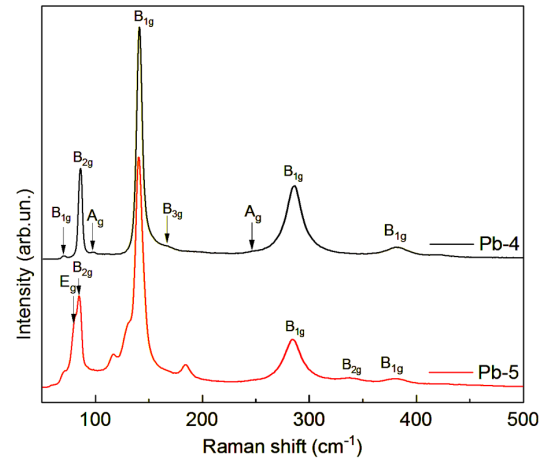
Fig. 3. Raman spectra of Pb-4 and Pb-5 powders; $\lambda_{exc} = 488.0$ nm, $T = 300$ K

them are acoustic vibrational modes, and the other nine are optical vibrational modes [26],

$$\Gamma_{\alpha-PbO} = A_{1g} + A_{2g} + B_{1g} + B_{2g} + 2E_g + $$
$$+ A_{1u} + A_{2u} + B_{2u} + 2E_u.$$

Two modes (A_{2u} and E_u) are active in the IR spectrum, and four vibrational modes (A_{1g}, B_{1g}, and $2E_g$) manifest themselves in the Raman spectra.

Orthorhombic β-PbO belongs to the space group $Pbcm$ (D_{2h}^{11}), which has four formula units in the unit cell. There are $3 \times 8 = 24$ phonon modes: 3 acoustic and 21 optical vibration modes [26],

$$\Gamma_{\beta\text{-}PbO} = 3B_{2u} + 4B_{1g} + 4A_g + 2B_{2g} + $$
$$+ 3B_{3u} + 2A_u + B_{1u} + 2B_{3g}.$$

The $3B_{2u}$, $3B_{3u}$, and B_{1u} vibrational modes are active in the IR spectra of β–PbO, whereas the $4B_{1g}$, $2B_{2g}$, $2B_{3g}$, and $4A_g$ vibrational modes reveal themselves in the Raman spectra. The $2A_u$ vibrational modes are the so-called "silent modes" because they do not appear in the IR and Raman spectra [27, 28].

In Fig. 3, the micro-Raman spectra of Pb-4 and Pb-5 powders are shown. They were registered at a low optical excitation power level ($P = 50$ kW/cm^2). Several phonon bands were registered in the Raman spectrum of specimen Pb–4: in particular, these are the bands at 70, 141, 285, and 381 cm^{-1}, which correspond to the B_{1g} phonon mode of orthorhombic β-PbO; the bands at 86 and 355 cm^{-1} are associated with the B_{2g} modes; the weak and broad band
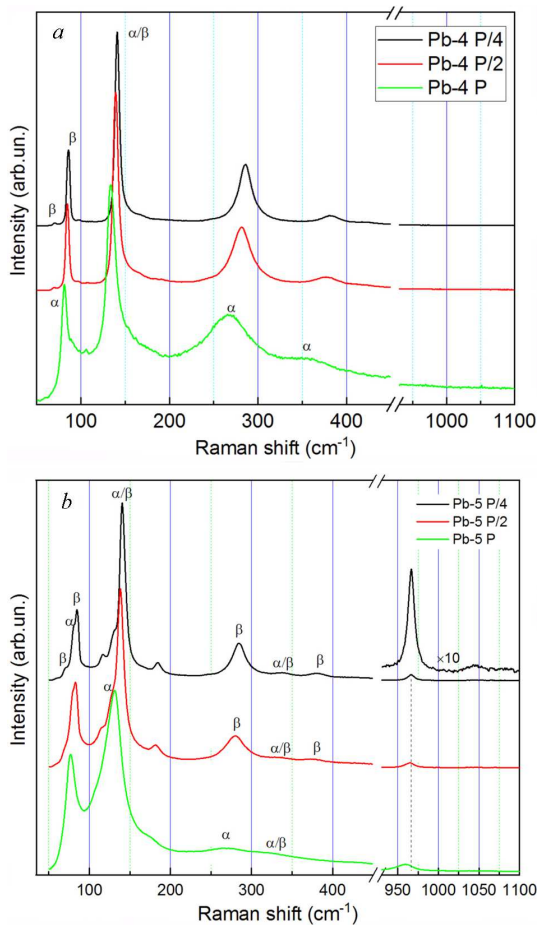
Fig. 4. Raman spectra of (*a*) Pb-4 and (*b*) Pb-5 powders at various optical excitation powers: 50 (P), 100 (P/2), and 200 kW/cm^2 (P/4); $\lambda_{exc} = 488.0$ nm. $T = 300$ K

at 168 cm^{-1} is attributed to the B_{3g} mode; and the weak bands at 97 and 279 cm^{-1} are associated with the A_g vibrational mode [28].

In the Raman spectrum of specimen Pb-4, in addition to the bands indicated above, an α-PbO mode at 84 cm^{-1} (it corresponds to A_g vibrations) and the B_{2u} vibration band at 337 cm^{-1} are also observed. They are quite close to the B_{2g} bands of β-PbO (at about 86 and 355 cm^{-1}) [27, 28].

The nature of the bands at 116, 131, and 184 cm^{-1} is unknown. Most probably, they are related to the scattering bands of lead carbonate nanoparticles. In paper [28], the authors studied natural PbCO$_3$ crystals and found Raman bands with rather close frequency positions. Indeed, the results of X-ray structural analysis testify to the presence of lead car-

bonate in the researched specimens. The unknown phonon bands described in work [29] may probably be of a similar origin, but this issue requires a further research.

The two- and fourfold growth of the optical excitation power (to 100 and 200 kW/cm^2, respectively) leads to changes in the shape, half-width, and position of the fundamental vibrational bands of powdered specimens (Fig. 4). Such a transformation may testify to a transition from orthorhombic β-PbO, which is unstable at room temperature, to stable tetragonal α-PbO. Simultaneously, the most intensive B_{1g} band in the spectra of both specimens becomes shifted: from 140 to 131 cm^{-1} for specimen Pb–5, and from 141 to 134 cm^{-1} for specimen Pb-4.

The frequency ratio between the Raman band observed at 286 cm^{-1} for the β-PbO phase and the band with a maximum at 337 cm^{-1} for the α-PbO phase [27] is a good indicator for determining the phase mixture of the studied material. This ratio can be used to obtain a qualitative information about the phase composition of researched specimens. It is worth noting that, besides the fundamental vibrational bands of $\alpha(\beta)$-PbO appearing in the Raman spectrum of specimen Pb-5, additional bands are also observed in the high-frequency spectral interval. These are an intensive band at 966 cm^{-1} and a weak broad band at 1044 cm^{-1}, both being associated with scattering in lead carbonate [28].

4. Conclusions

In this work, we have demonstrated a simple and effective method of open-cell electrochemical synthesis of PbO nanoparticles of two different modifications (α-PbO and β-PbO). It is demonstrated that the application of the NaCl solution as an electrolyte leads to the formation of a mixture of lead carbonate and two modifications of lead oxide, irrespective of the synthesis temperature. It is found that, as the synthesis temperature increases, the volume fraction of lead oxides in the examined specimens also increases. At the same time, the temperature growth leads to the formation of larger lead oxide nanoparticles and smaller lead carbonate nanoparticles. The results obtained for the phase distribution in the synthesized material from the study of Raman and PL spectra correlate well with the X-ray diffraction data. It is shown that the combination of the Raman and X-

ray diffraction methods to analyze a mixture of two PbO phases is more informative than the application of the X-ray diffraction alone owing to the overlap of the X-ray reflexes of the α- and β-PbO phases.

1. I.M. Trachtenberg, N.M. Dmitrukha, S.P. Lugovskyi, I.S. Chekman, V.O. Kuprii, A.M. Doroshenko. Lead is a dangerous pollutant. The old and new problem. *Suchas. Probl. Toksykol. Kharch..Khim. Bezpek.* **3**, 14 (2015) (in Ukrainian).

2. O. Grynko, T. Thibault, E. Pineau, A. Reznik. The X-ray sensitivity of an amorphous lead oxide photoconductor. *Sensors* **21**, 7321 (2021).

3. V.N. Suryawanshi, A.S. Varpe, M.D. Deshpande. Band gap engineering in PbO nanostructured thin films by Mn doping. *Thin Solid Films* **645**, 87 (2018).

4. Q. Li, C. Feng. Electrochemical performance of nanostructured PbO@C obtained by sol-gel method. *J. Electron. Mater.* **45**, 3127 (2016).

5. D.L. Perry, T.J. Wilkinson. Synthesis of high-purity α- and β-PbO and possible applications to synthesis and processing of other lead oxide materials. *Appl. Phys. A* **89**, 77 (2007).

6. O. Semeniuk, A. Csik, S. Kökéenyesi, A. Reznik. Ion-assisted deposition of amorphous PbO layers. *J. Mater. Sci.* **52**, 7937 (2017).

7. K.T. Arulmozhi, N. Mythili. Studies on the chemical synthesis and characterization of lead oxide nanoparticles with different organic capping agents. *AIP Advances* **3**, 122122 (2013).

8. S. Bratos, M. Wulff, J.-C. Leicknam, R. Vuilleumier, X. Rozanska. Visualizing chemical reactions with X-rays. *Ukr. J. Phys.* **56**, 763 (2022).

9. M. Torabi. Electrochemical evaluation of PbO nanoparticles as anode for lithium ion batteries (technical note). *Int. J. Eng.* **24**, 351 (2011).

10. O.Z. Didenko, P.E. Stryzhak, G.R. Kosmambetova, N.S. Kalchuk. Synthesis and morphology of low-dimensional quantum ZnO/MgO systems. *Fiz. Khim. Tverd. Tila* **10**, 106 (2009) (in Ukrainian).

11. N.B. Danilevska, M.V. Moroz, B.D. Nechyporuk, B.P. Rudyk. Preparation and properties of nanostructured ZnS and ZnO. *Zh. Mano-Electron. Fiz.* **8**, 01006 (2016) (in Ukrainian).

12. L.M. Kovba, V.K. Trunov. *X-ray Phase Analysis* (Moscow State Univ. Publ. House, 1976) (in Russian).

13. A.V. Lysytsia, M.V. Moroz, B.D. Nechyporuk, B.P. Rudyk, B.F. Shamsutdynov. Physical properties of nanocrystals of zinc compounds obtained using the electrolytic method. *Fiz. Khim. Tverd. Tila* **22**, 160 (2021) (in Ukrainian).

14. X. Zhu, L. Li, X. Sun, D. Yang, L. Gao, J. Liu, R.V. Kumar, J. Yang. Preparation of basic lead oxide from spent lead acid battery paste via chemical conversion. *Hydrometallurgy* **117–118**, 24 (2012).

15. X. Zhu, J. Yang, L. Gao, J. Liu, D. Yang, X. Sun, W. Zhang, Q. Wang, L. Li, D. He, R.V. Kumar. Preparation of lead carbonate from spent lead paste via chemical conversion. *Hydrometallurgy* **134–135**, 47 (2013).

16. N.B. Danilevska, M.V. Moroz, M.Yu. Novoseletskyi, B.P. Rudyk. The influence of technological regimes on the physical properties of zinc oxide nanocrystals obtained using the electrolytic method. *Zh. Fiz. Dosl.* **20**, 3601 (2016) (in Ukrainian)

17. A. Aliakbari, E. Najafi, M.M. Amini, S. Weng Ng. Structure and photoluminescence properties of lead(II) oxide nanoparticles synthesized from a new lead(II) coordination polymer. *Monatsh. Chem.* **145**, 1277 (2014)

18. B. Pathak, P.K. Kalita, N. Aomoa, J.P.R. Choudhury, H. Das. Shell induced optoelectronic characteristics of chemically synthesized PbO/ZnO core/shell nanocomposites for memcapacitive application. *Physica E* **139**, 115157 (2022)

19. H.J. Terpstra, R.A. de Groot, C. Haas. Electronic structure of the lead monoxides: Band-structure calculations and photoelectron spectra. *Phys. Rev. B* **52**, 11690 (1995)

20. V.A. Gaisin, D.S. Nedzvetskii, V.I. Filippov, N.Ya. Chistyakova, M.K. Sheinkman. *Opt. Spektrosk.* **48,** 775 (1980) (in Russian)

21. T.H. Matsumoto, K. Kato, M. Miyamoto, M. Sano, E.A. Zhukov, T. Yao. Correlation between grain size and optical properties in zinc oxide thin films. *Appl. Phys. Lett.* **81**, 1231 (2002)

22. H. Harad, Y. Sasa, M. Uda. Crystal data for β-PbO$_2$. *J. Appl. Crystallogr.* **14**, 141 (1981)

23. U. Houssermann, P. Berastegui, S. Carlson, J. Haines, J.-M. Leger. TlF and PbO under high pressure: Unexpected persistence of the stereochemically active electron pair. *Angew. Chem.* **113**, 4760 (2001)

24. P.B. Taunk, R. Das, D.P. Bisen, R.K. Tamrakar, N. Rathor. Synthesis and optical properties of chemical bath deposited ZnO thin film. *Int. J. Adv. Res. Sci. Eng.* **1**, 159 (2015)

25. H. Giefers, F. Porsch. Shear induced phase transition in PbO under high pressure. *Physica B* **400**, 53 (2007)

26. P. Canepa, P. Ugliengo, M. Alfredsson. Elastic and vibrational properties of α- and β-PbO. *J. Phys. Chem. C*, **116**, 21514 (2012)

27. G.L.J. Trettenhahn, G.E. Nauer, A. Neckel. Vibrational spectroscopy on the PbO-PbSO$_4$ system and some related compounds: Part 1. Fundamentals, infrared and Raman spectroscopy. *Vibr. Spectrosc.* **5**, 85 (1993)

28. R.L. Frost, W. Martens, J.T. Kloprogge, Z. Ding. Raman spectroscopy of selected lead minerals of environmental significance. *Spectrochim. Acta A* **59**, 2705 (2003)

29. O. Kapush, N. Mazur, A. Lysytsya, M.V. Moroz, B.D. Nechyporuk, B.P. Rudyk, V.M. Dzhagan, M.Ya. Valakh, V.O. Yukhymchuk. Physical properties of nanocrystalline PbS synthesized by electrolytic method. *Phys. Chem. Solid State* **24**, 262 (2023).

Б.Д. Нечипорук, О.Ф. Коломис,
Б.П. Рудик, В.В. Стрельчук, М.В. Мороз,
В.О. Мислінчук, Б.А. Татарин

ОПТИЧНІ ТА СТРУКТУРНІ
ВЛАСТИВОСТІ НАНОПОРОШКІВ
СПОЛУК СВИНЦЮ, ОТРИМАНИХ
ЕЛЕКТРОЛІТИЧНИМ МЕТОДОМ

Досліджено вплив температури та складу електроліту на процес отримання нанопорошків сполук свинцю електролітичним методом з використанням свинцевих електродів. Проведено рентґеноструктурні дослідження, результати яких було використано для визначення складу отриманих зразків та розмірів нанокристалів за допомогою формули Дебая–Шеррера. Обговорюються можливості утворення оксидів свинцю і карбонату свинцю при використанні електролітичного методу отримання наночастинок. Показано, що незалежно від температури електроліту отримуються нанокристали оксиду і карбонату свинцю. Результати рентґеноструктурних досліджень цих зразків порівнюються з результатами комбінаційного розсіювання світла (КРС). Проведено аналіз смуг фотолюмінесценції сформованих сполук.

К л ю ч о в і с л о в а: α-, β-оксид свинцю, карбонат свинцю, рентґеноструктурні дослідження, розміри наночастинок, формула Дебая–Шеррера, комбінаційне розсіювання світла, фотолюмінесценція.